Article

Cell Metabolism

Reversal of Mitochondrial Transhydrogenase Causes Oxidative Stress in Heart Failure

Graphical Abstract

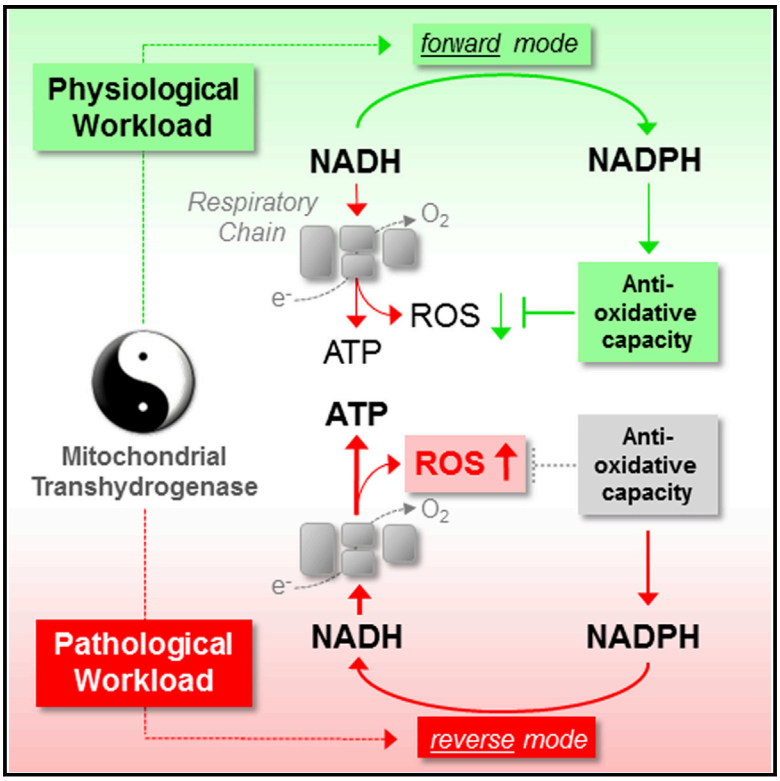

Highlights

- Mitochondrial transhydrogenase (Nnt) normally regenerates NADPH from NADH
- Pathologic workload reverses Nnt to deplete NADPH and antioxidative capacity
- Reverse Nnt induces mitochondrial oxidative stress and necrosis
- Defective Nnt in C57BL/6J mice ameliorates pressure overload-induced heart failure

Authors

Alexander G. Nickel, Albrecht von Hardenberg, Mathias Hohl, ..., Michael Böhm, Markus Hoth, Christoph Maack

Correspondence

christoph.maack@uks.eu

In Brief

The mitochondrial transhydrogenase (Nnt) normally regenerates NADPH from NADH to bolster antioxidative capacity. Nickel et al. show that pathological workload reverses the Nnt reaction and depletes NADPH in the mouse heart, which increases ROS production and leads to maladaptive cardiac remodeling in heart failure.

Nickel et al., 2015, Cell Metabolism *22*, 472–484
September 1, 2015 ©2015 Elsevier Inc.
http://dx.doi.org/10.1016/j.cmet.2015.07.008

CellPress

Cell Metabolism
Article

Reversal of Mitochondrial Transhydrogenase Causes Oxidative Stress in Heart Failure

Alexander G. Nickel,[1] Albrecht von Hardenberg,[1] Mathias Hohl,[1] Joachim R. Löffler,[1] Michael Kohlhaas,[1] Janne Becker,[1] Jan-Christian Reil,[1] Andrey Kazakov,[1] Julia Bonnekoh,[1] Moritz Stadelmaier,[1] Sarah-Lena Puhl,[1] Michael Wagner,[1] Ivan Bogeski,[2] Sonia Cortassa,[3] Reinhard Kappl,[2] Bastian Pasieka,[2] Michael Lafontaine,[4] C. Roy D. Lancaster,[4] Thomas S. Blacker,[5,6] Andrew R. Hall,[7] Michael R. Duchen,[5] Lars Kästner,[8] Peter Lipp,[8] Tanja Zeller,[9,10] Christian Müller,[9,10] Andreas Knopp,[1] Ulrich Laufs,[1] Michael Böhm,[1] Markus Hoth,[2] and Christoph Maack[1,*]

[1]Klinik für Innere Medizin III, Universitätsklinikum des Saarlandes, 66421 Homburg, Germany
[2]Department of Biophysics, CIPMM, School of Medicine, Saarland University, 66421 Homburg, Germany
[3]Johns Hopkins University, Baltimore, MD 21218, USA
[4]Department of Structural Biology, Saarland University, 66421 Homburg, Germany
[5]Department of Cell and Developmental Biology
[6]Department of Physics and Astronomy
[7]The Hatter Cardiovascular Institute
University College London, London WC1E 6BT, UK
[8]Institut für Zellbiologie, Universität des Saarlandes, 66421 Homburg, Germany
[9]Klinik für Allgemeine und Interventionelle Kardiologie, Universitäres Herzzentrum Hamburg, 20246 Hamburg, Germany
[10]Deutsches Zentrum für Herzkreislaufforschung (DZHK e.V.), Partner Site Hamburg/Lübeck/Kiel, Germany
*Correspondence: christoph.maack@uks.eu
http://dx.doi.org/10.1016/j.cmet.2015.07.008

SUMMARY

Mitochondrial reactive oxygen species (ROS) play a central role in most aging-related diseases. ROS are produced at the respiratory chain that demands NADH for electron transport and are eliminated by enzymes that require NADPH. The nicotinamide nucleotide transhydrogenase (Nnt) is considered a key antioxidative enzyme based on its ability to regenerate NADPH from NADH. Here, we show that pathological metabolic demand reverses the direction of the Nnt, consuming NADPH to support NADH and ATP production, but at the cost of NADPH-linked antioxidative capacity. In heart, reverse-mode Nnt is the dominant source for ROS during pressure overload. Due to a mutation of the *Nnt* gene, the inbred mouse strain C57BL/6J is protected from oxidative stress, heart failure, and death, making its use in cardiovascular research problematic. Targeting Nnt-mediated ROS with the tetrapeptide SS-31 rescued mortality in pressure overload-induced heart failure and could therefore have therapeutic potential in patients with this syndrome.

INTRODUCTION

While mitochondria are the major source of cellular ATP, they can also emerge as important generators of reactive oxygen species (ROS) (Balaban et al., 2005; Murphy, 2009). Increased mitochondrial ROS production plays an important role in aging (Schriner et al., 2005) and many aging-related diseases, including neurodegenerative (Lin and Beal, 2006), metabolic (Lee et al., 2010), and cardiac diseases (Dai et al., 2009). Chronic heart failure is the most frequent cause of hospitalization in persons aged ≥65 years and commonly results from myocardial infarction and/or hypertension (Roger, 2013), and in both scenarios, mitochondrial ROS contribute to deterioration of cardiac function (Dai et al., 2012; Matsushima et al., 2006). In heart, ROS impair excitation-contraction coupling, cause arrhythmias (Wagner et al., 2013), activate prohypertrophic signaling (Ago et al., 2008), and induce apoptotic and/or necrotic cell death through activation of the permeability transition pore (PTP) (Halestrap, 2005). Recent advances in pharmacology targeting mitochondrial ROS production provide novel therapeutic options in a broad spectrum of diseases (Smith et al., 2012; Szeto, 2014) and require a precise understanding of the regulation of mitochondrial ROS production in physiology and disease.

The heart is an organ with uniquely high demands of ATP. During exercise, ATP production can increase ~4-fold, requiring efficient adaptation of respiration through ADP and Ca^{2+} (Balaban, 2002; Cortassa et al., 2006). A physiological increase in workload is triggered by β-adrenergic stimulation, which increases ADP (through ATP hydrolysis) and at the same time, cytosolic Ca^{2+} (Figure 1A). While ADP accelerates respiration and oxidizes NADH to NAD^+ by stimulating ATP production at the F_1F_o-ATP synthase, Ca^{2+} enters mitochondria and activates Krebs cycle dehydrogenases to regenerate NADH. This "parallel activation" of respiration maintains constant ratios of ATP/ADP and NADH/NAD^+ over a wide range of physiological workloads (Balaban, 2002).

We discovered recently that mitochondrial Ca^{2+} uptake is also important to maintain NADPH for the elimination of hydrogen peroxide (H_2O_2), since all enzymes that regenerate mitochondrial NADPH derive their substrates from the Krebs cycle (Kohlhaas et al., 2010) (Figure 1A). In heart failure, disturbed Ca^{2+} and Na^+ handling hamper mitochondrial Ca^{2+} uptake and thus, provoke NADH and NADPH oxidation and mitochondrial ROS

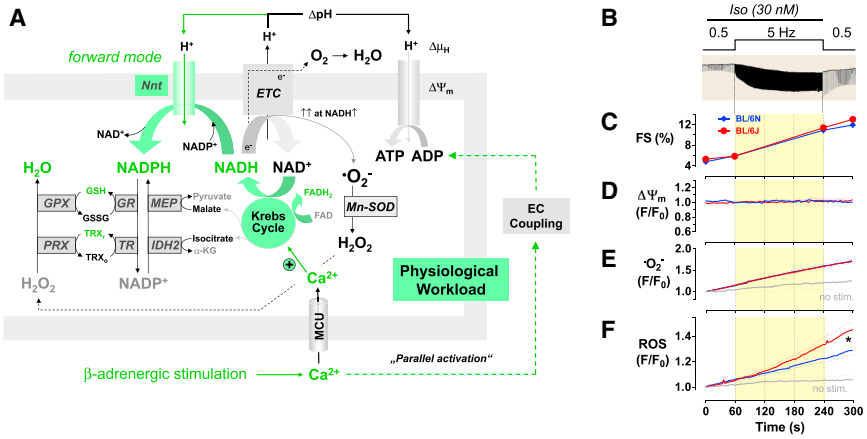

Figure 1. Nnt Contributes to Antioxidative Capacity during β-Adrenergic Stimulation

(A) Mitochondrial NADPH regeneration is accomplished by $NADP^+$-dependent isocitrate-dehydrogenase 2 (IDH2), malic enzyme (MEP), and the Nnt. GR, glutathione reductase; TR, thioredoxin reductase; MCU, mitochondrial Ca^{2+} uniporter.

(B) Isolated myocytes from BL/6N and BL/6J mice were electrically stimulated at 0.5 Hz and then exposed to isoproterenol (30 nM) and stimulation frequency increased to 5 Hz. Stimulation protocol and representative trace of cell length.

(C–F) Systolic sarcomere shortening (C), mitochondrial membrane potential ($\Delta\Psi_m$; by TMRM) (D), mitochondrial $\bullet O_2^-$ (by MitoSOX) (E), and cellular ROS (by CM-H_2DCFDA) (F) during the protocol.

Data are presented as means ± SEM. *$p < 0.05$ BL/6N versus BL/6J. See also Figure S1.

emission (Kohlhaas et al., 2010). These and other studies led to the concept of "redox-optimized ROS balance" (Aon et al., 2010), which implies that both production of superoxide ($\bullet O_2^-$) at the electron transport chain (ETC; fueled by NADH) and elimination of H_2O_2 (by NADPH-dependent enzymes) are favored by reduced redox states (Figure 1A). In this scenario, mitochondria are optimized to maximize energy output while keeping H_2O_2 overflow to a minimum by operating in an intermediate redox state, while extreme oxidation or reduction can induce oxidative stress (Aon et al., 2010).

The nicotinamide nucleotide transhydrogenase (Nnt) is at the critical interface between the NADH and NADPH pools in mitochondria, and despite a high abundance in the heart, its precise role for the regulation of mitochondrial ROS production and elimination is not well understood. The Nnt catalyzes the reaction $NADH^+NADP^+ \leftrightarrow NADPH^+NAD^+$ and is coupled to the protonmotive force ($\Delta\mu_H$; Figure 1A). Since high $\Delta\mu_H$ in energized mitochondria favors NADPH production, the Nnt is deemed to be a key antioxidative enzyme (Rydström, 2006). Recently, it was discovered that C57BL/6 mice from The Jackson Laboratories (BL/6J) have a loss-of-function mutation in the gene encoding the Nnt by the missense of exons 7–11, accounting for glucose intolerance of this strain (Toye et al., 2005). In pancreatic islet cells exposed to high glucose, deletion of the Nnt led to oxidative stress and impaired ATP production and insulin release (Freeman et al., 2006; Toye et al., 2005). Furthermore, BL/6J mice are more sensitive to deletion of Mn^{2+}-dependent superoxide dismutase (Mn-SOD) than other strains by developing cardiomyopathy, which was also related to the *Nnt* mutation (Huang et al., 2006) and ameliorated by re-expressing one wild-type *Nnt* allele in BL/6J mice (Kim et al., 2010).

Here, we report that opposite to this prevailing view of the Nnt as an antioxidative enzyme, it switches to a pro-oxidative mode in situations of pathologic cardiac workload by reversing its direction, oxidizing NADPH to regenerate NADH for ATP production, but at the cost of the NADPH-dependent antioxidative capacity. This reverse-mode Nnt reaction increases mitochondrial ROS emission and accounts for maladaptive cardiac remodeling and mortality in response to pressure overload, while BL/6J mice lacking a functional *Nnt* are protected from heart failure. Since BL/6J is the most commonly used mouse strain in biomedical research, these data indicate that in numerous studies that applied cardiac pressure overload in this strain, oxidative stress was systematically underestimated. Our results further emphasize the importance of mitochondrial ROS production for the progression of heart failure and the feasibility of targeting mitochondria to protect the heart from remodeling and contractile dysfunction.

RESULTS

Expression and Activity of Nnt and Other NADPH-Regenerating Enzymes

In agreement with previous studies, exons 7–11 of the gene encoding Nnt were missing in BL/6J, but not BL/6N mice (Huang et al., 2006) (Figure S1A). In BL/6N mice, Nnt protein expression was highest in the heart, moderate in kidney and liver but absent from brain and skeletal muscle (Figure S1B). In heart, Nnt was expressed in myocytes and fibroblasts (Figures S1C and S1D). In contrast, Nnt expression was absent from any tissue in BL/6J mice (Figures S1B and S1C). Accordingly, Nnt enzymatic activity was detected in cardiac, but hardly in brain- and not in skeletal muscle mitochondria from BL/6N mice, while it was zero in any mitochondria in BL/6J mice (Figure S1E).

Since mitochondrial NADPH can be regenerated not only by the Nnt, but also by isocitrate dehydrogenase (IDH2) and malic enzyme (MEP) (Figure 1A), we ruled out a compensatory upregulation of these enzymes in BL/6J mitochondria (Figures S1F and S1G). Based on their NADPH-regenerating efficacies, IDH2 has the highest contribution to overall NADPH regenerating capacity in cardiac BL/6N mitochondria (~70%), followed by Nnt (~22%) and MEP (8%; Figure S1H).

The *Nnt* mutation in BL/6J was originally discovered by this strain's impaired glucose tolerance (Toye et al., 2005). As the underlying mechanism, glucose-induced oxidative stress in pancreatic beta cells was reported (Freeman et al., 2006). Therefore, we compared Nnt activity to IDH2 and MEP activities in pancreatic islets of BL/6N and BL/6J mice. In the presence of ATP, which resembles the situation when glucose induces insulin release, IDH2 activity was largely suppressed (Figure S1I). No relevant amounts of MEP activity were detected under either condition (not shown). In the presence of ATP, Nnt activity was

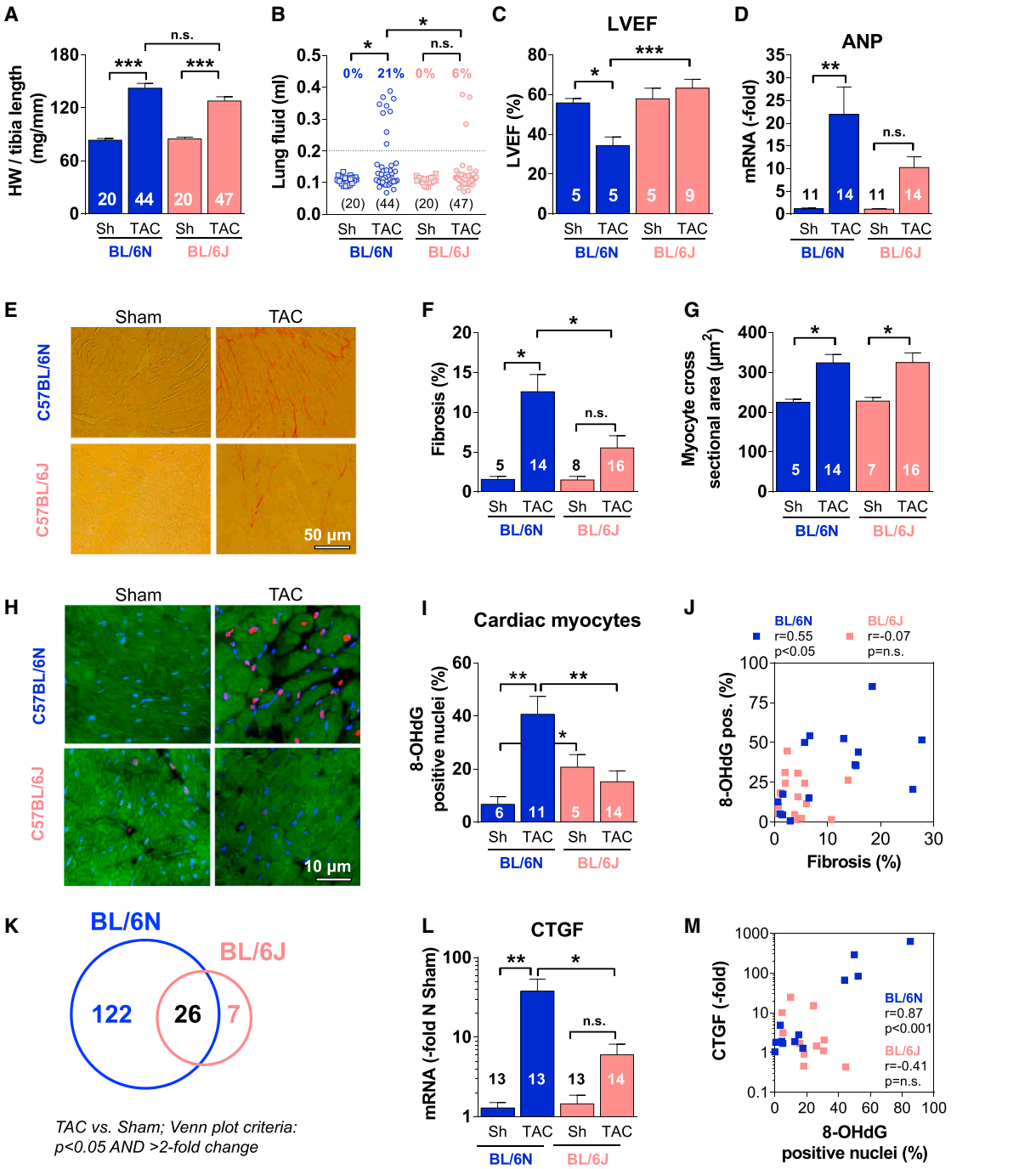

Figure 2. Ameliorated Cardiac Remodeling and Oxidative Stress in BL/6J Compared to BL/6N Mice

BL/6N and BL/6J mice were exposed to TAC or sham-surgery for 6 weeks.

(A) Heart weight (HW) to tibia length ratio.

(B) Lung fluid; pulmonary congestion was defined as >0.2 ml. The percentages indicate the fraction above this threshold. *p < 0.05 (Fisher's exact test).

(C) LV ejection fraction (LVEF) determined in isolated working hearts.

(D) LV expression of *ANP* mRNA.

(E) Representative histological images of fibrosis in LV myocardium.

(F) Quantification of fibrosis.

(G) Quantification of myocyte cross-sectional area in the LV.

(H) Representative 8-OHdG staining of LV nuclei as index for intracellular ROS.

(I) Quantification of 8-OHdG staining in LV cardiac myocytes.

(J) Correlation between 8-OHdG staining and fibrosis.

(legend continued on next page)

higher than IDH2 activity and therefore the dominating enzyme with NADPH-regenerating capacity under these conditions (Figures S1I and S1J).

Nnt Contributes to NADPH Regeneration and ROS Elimination during a Physiological Workload Increase

To examine the functional consequences of Nnt deficiency for mitochondrial ROS formation, isolated cardiac myocytes were exposed to the β-adrenergic agonist isoproterenol and an increased stimulation rate (Figure 1B). This induced similar increases of sarcomere shortening, cytosolic and mitochondrial Ca^{2+} without any differences between BL/6N and BL/6J myocytes (Figures 1B, 1C, and S1K–S1L). Furthermore, $\Delta\Psi_m$ remained stable during the protocol without differences between strains (Figure 1D). Electrical stimulation per se increased mitochondrial ROS formation (Figures 1E and 1F). While no differences in $\bullet O_2^-$ formation were observed between strains, H_2O_2 (and presumably also other ROS due to the limited specificity of DCF to H_2O_2) increased in BL/6J versus BL/6N myocytes during the workload transition (Figures 1E and 1F). These data are in agreement with the concept that during a physiological increase in workload triggered by β-adrenergic stimulation, the Nnt contributes to NADPH regeneration to fuel H_2O_2-detoxifying enzymes (Figure 1A).

Ameliorated Cardiac Remodeling in BL/6J versus BL/6N Mice after Pressure Overload

Since mitochondrial ROS production plays an important role for cardiac remodeling in response to pressure overload (Dai et al., 2012), we speculated that the lack of Nnt in BL/6J mice should aggravate the development of heart failure 6 weeks after transverse-aortic constriction (TAC). However, TAC led to similar increases in heart weight in both strains (Figure 2A), and against our expectations, pulmonary congestion (indicating cardiac decompensation) was more frequent in BL/6N than in BL/6J mice (Figure 2B). Isolated working heart analyses revealed decreased left ventricular (LV) ejection fraction (Figure 2C) and elevated LV volume at 70 mmHg end-systolic pressure (integrating systolic dysfunction with LV enlargement; Figure S2A) in BL/6N, but not BL/6J mice after TAC. Accordingly, mRNA expression of atrial natriuretic peptide (*ANP*), an index of LV filling pressures, was substantially increased after TAC in BL/6N and ameliorated in BL/6J mice (Figure 2D). Also, the increase in LV fibrosis was more pronounced in BL/6N than BL/6J mice (Figures 2E and 2F) despite similar increases in myocyte cross sectional area (Figure 2G).

To understand the underlying mechanisms for these unexpected results, we analyzed nuclear staining of 8-hydroxy-2′-deoxyguanosine (8-OHdG) in LV myocardium as an indicator of intracellular ROS formation. In sham-operated animals, 8-OHdG staining was slightly elevated in BL/6J compared to BL/6N mice (Figures 2H and 2I). In stark contrast, TAC substantially increased 8-OHdG staining in myocytes and non-myocytes from BL/6N, but not BL/6J hearts (Figures 2H, 2I, and S2B). The levels of oxidative stress correlated with the degree of fibrosis, cardiac hypertrophy, *ANP* upregulation, and pulmonary congestion in BL/6N mice ($p < 0.01$, respectively), while these correlations were lost in BL/6J mice (Figure 2J and data not shown).

To gain further insight into the mechanisms of remodeling, we performed gene array analyses. When applying a p value of <0.05 and a threshold of at least a 2-fold change, 148 genes were differentially regulated by TAC versus sham in BL/6N mice, while only 33 genes were differentially regulated in BL/6J mice (Figure 2K; Tables S1 and S2). Of these 33 genes, 26 were also regulated in BL/6N mice (Figure 2K), indicating similar, but clearly ameliorated TAC-induced genomic remodeling in BL/6J mice. Accordingly, pathway analyses revealed upregulation of cardiac hypertrophy and fibrosis pathways in BL/6N ($p < 0.001$, respectively; data not shown), but not BL/6J mice after TAC.

Of the fibrotic pathways, the most consistent change in BL/6N mice after TAC was of the gene encoding connective tissue growth factor (CTGF), which is inducible by H_2O_2 (Park et al., 2001). Real-time PCR confirmed strong upregulation of *CTGF* after TAC in BL/6N, which was blunted in BL/6J mice (Figure 2L). *CTGF* upregulation correlated closely with oxidative stress in hearts from BL/6N, but not BL/6J mice (Figure 2M). In contrast, other genes involved in fibrosis were not differentially regulated (Figures S2C and S2D).

An Unexpected Yin-Yang Role of the Nnt for the Regulation of Mitochondrial ROS

The analyses of 8-OHdG in LV myocardium (Figures 2H and 2I) indicate that in response to a pathological increase in cardiac afterload, oxidative stress is more pronounced in BL/6N than in BL/6J mice. Given that the Nnt is viewed as an antioxidative enzyme (Rydström, 2006), supported by our results in cardiac myocytes during a physiological workload transition (Figures 1A and 1F), this appeared paradoxical. Thus, we challenged our initial hypothesis and reasoned that under different metabolic conditions, the direction of the Nnt reaction may vary. A physiological workload transition (triggered by β-adrenergic activation) increases Ca^{2+} and activates the Krebs cycle, compensating the ETC-induced oxidation of NADH ("parallel activation"; Figure 1A) (Cortassa et al., 2006; Maack et al., 2006). In contrast, when increasing preload in isolated cardiac trabeculae, contractile force (and consequently ATP consumption) increase via the Frank Starling mechanism without a parallel increase in Ca^{2+} (Backx and Ter Keurs, 1993). Accordingly, increasing preload in cardiac trabeculae oxidizes NAD(P)H to $NAD(P)^+$ without a compensatory Ca^{2+}-induced regeneration (Brandes and Bers, 1997). We therefore reasoned that the in vitro conditions in un-stretched myocytes performing low levels of mechanical work, but with high Ca^{2+}-stimulated Krebs cycle activity (Figure 1) may be opposite to the in vivo conditions after TAC, with high mechanical workload without Ca^{2+}-induced "parallel activation" of the Krebs cycle.

(K) Venn plot diagram indicating the numbers of genes changed after TAC versus sham in BL/6N and BL/6J mice, applying a $p < 0.05$ and >2-fold change.
(L) mRNA expression of *CTGF* in the LV.
(M) Correlation between *CTGF* expression and 8-OHdG staining.
Data are presented as means ± SEM. *$p < 0.05$, **$p < 0.01$, and ***$p < 0.0001$ (one-way ANOVA, Tukey's post test). Replicates (n) are displayed as numbers in the columns. See also Figure S2.

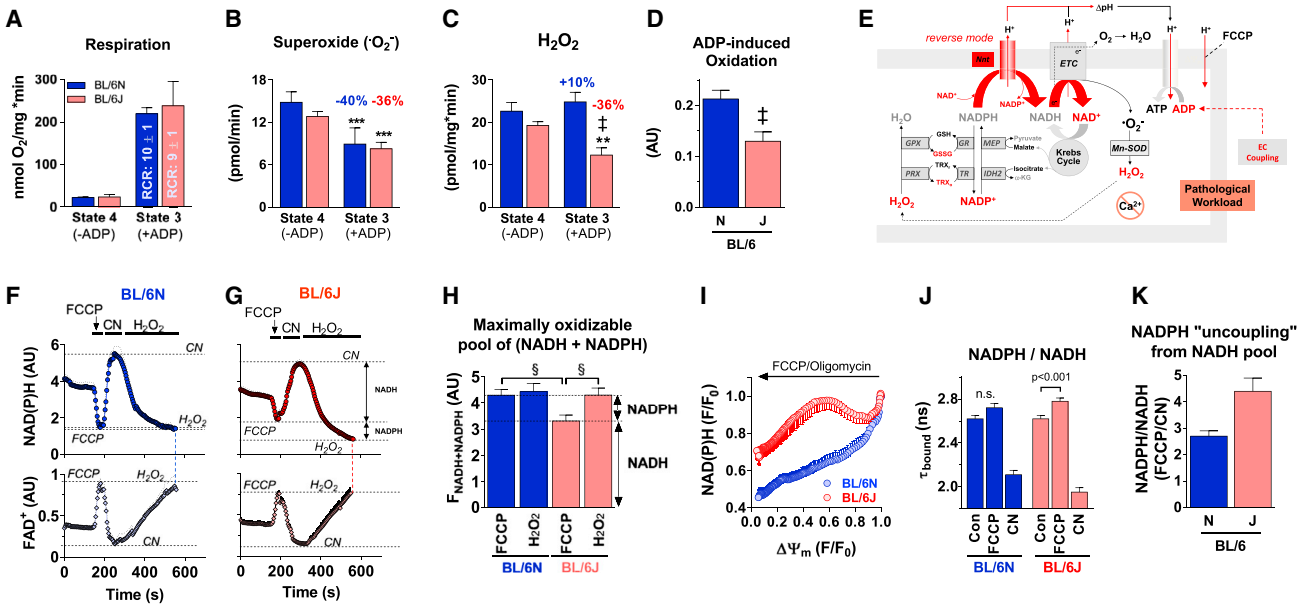

Figure 3. Accelerating Respiration Induces Reverse-Mode Nnt Reaction

(A) O_2 consumption in isolated cardiac mitochondria supplied with pyruvate/malate (5/5 mM) in the absence (State 4) and presence of ADP (1 mM; State 3). RCR, respiratory control ratio.

(B) Mitochondrial $\bullet O_2^-$ formation determined by EPR.

(C) Mitochondrial emission of H_2O_2 determined by Amplex Ultra-Red.

(D) ADP-induced oxidation of NAD(P)H autofluorescence. AU, arbitrary units.

(E) Accelerating NADH-coupled respiration (by ADP or FCCP) induces reverse-mode Nnt, oxidizing NADPH, GSH, and TRX/PRX, and increasing H_2O_2 emission.

(F and G) Autofluorescence of NAD(P)H/NAD(P)$^+$ and $FADH_2$/FAD in isolated cardiac myocytes from BL/6N (F) and BL/6J (G) mice exposed to FCCP (5 μM), cyanide (4 mM), and H_2O_2 (10 mM), respectively.

(H) Quantification of the FCCP- and H_2O_2-sensitive pools of NAD(P)H/NAD(P)$^+$, calculated from data in (F) and (G).

(I) NAD(P)H plotted against $\Delta\Psi_m$ in response to FCCP/oligomycin.

(J) Fluorescence decay rate (τ_{bound}) of NAD(P)H reporting bound NADPH/NADH in the absence (Con; n = 5, 21 images) and presence of FCCP (5 μM; n = 3, 16 images) or cyanide (4 mM; n = 1, 8 images), respectively.

(K) NADPH/NADH during FCCP divided by NADPH/NADH during cyanide as an index for NADPH uncoupling from the NADH pool.

Data are presented as means ± SEM. $^{**}p < 0.01$, $^{***}p < 0.001$ versus State 4 (paired t test). †$p < 0.05$, ‡$p < 0.01$ versus BL/6 (unpaired t test). §$p < 0.05$ (one-way ANOVA, Tukey's post test). See also Figure S3.

To simulate such a pathological workload transition, we applied ADP to isolated cardiac mitochondria in the absence of Ca^{2+}. In agreement with the prevailing paradigm of mitochondrial ROS production (Balaban et al., 2005), ADP accelerated O_2 consumption and lowered $\bullet O_2^-$ formation (detected by EPR spin trap), without any differences between strains (Figures 3A and 3B). In contrast, ADP did not reduce H_2O_2 emission from BL/6N mitochondria (detected by Amplex Ultra-Red assay), whereas in BL/6J mitochondria, H_2O_2 emission was reduced by a similar degree as $\bullet O_2^-$ formation (by 36%, respectively; Figures 3B and 3C). Indeed, this was opposite to the results in isolated myocytes exposed to β-adrenergic stimulation (Figure 1F), where ROS emission was higher in BL/6J than in BL/6N myocytes. In contrast, in mitochondria from brain and skeletal muscle of BL/6N mice, in which no Nnt activity was detected (Figure S1E), ADP lowered H_2O_2 emission to a similar extent as $\bullet O_2^-$ without differences between strains (Figures S3A–S3F).

Reverse-Mode Nnt Oxidizes NADPH when Respiration Is Accelerated

Based on these opposing observations, we formulated the following hypothesis: accelerating respiration with ADP oxidizes NADH, and if NADH is not sufficiently regenerated by the Krebs cycle, NAD^+ provides a substrate for the reverse reaction of the Nnt, which is further facilitated by high NADPH, low NADH, and ADP-induced dissipation of $\Delta\mu_H$ (Figure 3E). This reversal of the Nnt oxidizes NADPH to regenerate NADH, which is consumed by the ETC. In fact, oxidation of the overall NAD(P)H/NAD(P)$^+$ redox pool by ADP was more pronounced in BL/6N than BL/6J mitochondria (Figure 3D).

To interrogate this further, we measured mitochondrial NAD(P)H/NAD(P)$^+$ and $FADH_2$/FAD redox states in isolated cardiac myocytes and exposed them to the uncoupler FCCP, the complex IV inhibitor cyanide and external H_2O_2 (Figure 3F). Similar to ADP, FCCP accelerates respiration (by dissipating $\Delta\mu_H$) and thereby oxidizes NADH. While cyanide completely reduced the redox states of NAD(P)H/NAD(P)$^+$ and $FADH_2$/FAD, H_2O_2 completely oxidized both NADPH and NADH independent of the presence of Nnt.

In fact, FCCP led to an identical oxidation of the overall NAD(P)H/NAD(P)$^+$ redox pool as H_2O_2 in BL/6N myocytes (Figure 3F). In contrast, in BL/6J myocytes, the oxidation of NAD(P)H/NAD(P)$^+$ by FCCP was less pronounced than by H_2O_2 and less than by FCCP in BL/6N myocytes (Figures 3F and 3G). The redox state

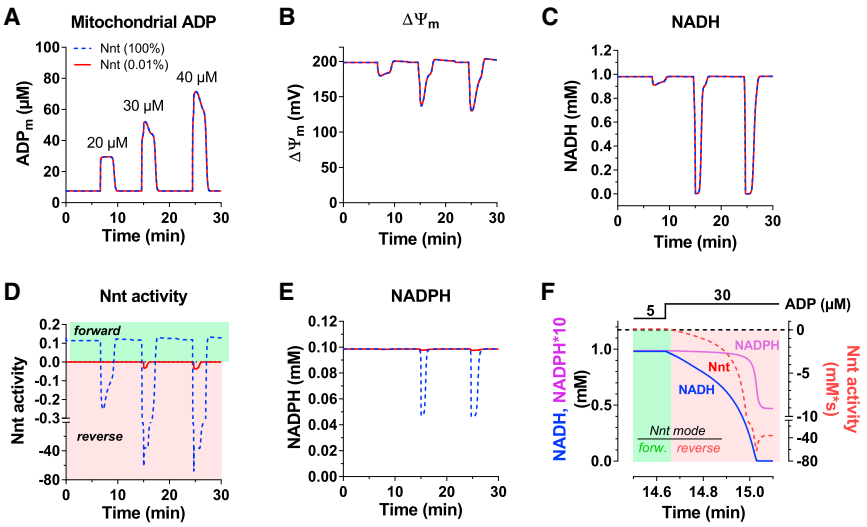

Figure 4. Computational Modeling Indicates Reversal of Nnt during NADH Oxidation

(A–E) A computational two-compartment model (Kembro et al., 2013) integrating mitochondrial energetics with redox regulation was used to assess the effect of transient increases in extra-mitochondrial ADP from 5 to 20, 30, and 40 μM ADP, respectively, on (A) mitochondrial [ADP], (B) $\Delta\Psi_m$, (C) mitochondrial [NADH], (D) Nnt activity, and (E) mitochondrial [NADPH].

(F) Changes in [NADH] and [NADPH] together with Nnt activity in response to a step increase from 5 to 30 μM [ADP] at higher temporal resolution.

Green/red shaded areas indicate forward/reverse-mode Nnt activity, respectively.

of $FADH_2$/FAD in the same cells (Figures 3F and 3G, lower traces) served to control for the redox state of the ETC, which should parallel the behavior of NADH (but not NADPH). These results suggest that despite FCCP-induced oxidation of NADH, NADPH is conserved in BL/6J mitochondria in the absence of a reverse-mode Nnt reaction. Maintained NADPH (and H_2O_2 eliminating capacity) in BL/6J mitochondria during accelerated NADH-coupled respiration could explain why in the presence of ADP, H_2O_2 was lowered by the same degree as $\bullet O_2^-$ in isolated mitochondria (i.e., by 36%; Figures 3B and 3C). Comparison of the absolute H_2O_2- and FCCP-sensitive fluorescence of the NAD(P)H/NAD(P)$^+$ redox pool indicates that (1) the pool sizes per se were not different between BL/6N and BL/6J mitochondria, and (2) NADPH contributes ~23% and NADH ~77% to this fluorescence (Figure 3H).

Since the Nnt is coupled to $\Delta\mu_H$, a reversal of the Nnt should also reverse the direction of proton translocation across the inner mitochondrial membrane, thereby possibly contributing to $\Delta\Psi_m$ (Figure 3E). In fact, when accelerating respiration in isolated myocytes with FCCP, $\Delta\Psi_m$ dissipated slightly faster in BL/6J than in BL/6N myocytes (Figures S3G and S3H), indicating that reverse-mode Nnt might delay dissipation of $\Delta\Psi_m$ by consuming NADPH. Similar results were obtained when Nnt was inhibited acutely with a chemical inhibitor (NBD-chloride) in BL/6N myocytes (Figures S3I and S3J). Despite this slight delay, $\Delta\Psi_m$ was dissipated by similar extents in myocytes from BL/6N and BL/6J mice. In agreement with this, steady-state $\Delta\Psi_m$ was unchanged in isolated and energized BL/6N and BL/6J mitochondria after titration of the uncoupler DNP, in the absence or presence of nigericin (that dissipates ΔpH, but not $\Delta\Psi_m$; Figures S3K and S3L), suggesting that the overall contribution of reverse-mode Nnt to $\Delta\Psi_m$ is rather small.

In isolated cardiac myocytes, for any given $\Delta\Psi_m$ during FCCP-induced dissipation, the redox state of NAD(P)H/NAD(P)$^+$ remained more reduced in BL/6J than in BL/6N mitochondria (Figure 3I), further supporting that Nnt-deficiency may maintain NADPH during accelerated respiration. To test this further, we employed fluorescence lifetime imaging (FLIM), where the longer time constant of NAD(P)H fluorescence decay (τ_{bound}) reflects the ratio of bound NADPH to NADH (Blacker et al., 2014). In agreement with previous data on HEK cells, FCCP did not change τ_{bound} in BL/6N myocytes (Figure 3J), since NADH and NADPH are oxidized by FCCP to similar extents, presumably through equilibration of both pools via the Nnt (Blacker et al., 2014). In contrast, FCCP caused a small but significant increase in τ_{bound} in BL/6J myocytes, indicating more pronounced oxidation of NADH than NADPH (Figure 3J). Vice versa, blocking the ETC with cyanide reduces the redox state of NADH, and since the total pool of NADH is larger than the NADPH pool, τ_{bound} shifts further toward the value predicted for purely NADH (~1.5 ns; Figure 3J). This was even more pronounced in BL/6J myocytes, where a lack of forward-mode Nnt may hinder complete NADPH reduction. Therefore, when dividing the estimated NADPH/NADH ratios after FCCP by the ratios after cyanide, respectively, the greater values in BL/6J myocytes indicate that the NADPH pool is more "uncoupled" from the NADH pool (compared to BL/6N; Figure 3K), consistent with a lack of Nnt-mediated equilibration of NADH and NADPH pools in either direction and supporting the idea that NADPH is relatively conserved after oxidation of NADH by FCCP.

Furthermore, we performed computational modeling using a two-compartment model that integrates mitochondrial energetics with redox regulation (Kembro et al., 2013). Starting from low extra-mitochondrial [ADP] of 5 μM, transient increases of [ADP] to 20, 30, and 40 μM increased mitochondrial [ADP] (Figure 4A), dissipated $\Delta\Psi_m$ and oxidized NADH (Figures 4B and 4C). While at low [ADP], the Nnt operated in the forward mode, it reversed direction during NADH oxidation, inducing NADPH oxidation (Figures 4D and 4E). Reducing Nnt activity 10,000-fold prevented NADPH oxidation (Figure 4E) despite similar NADH oxidation and $\Delta\Psi_m$ dissipation (Figures 4B and 4C). Of note, the Nnt reverses already early after initiation of NADH oxidation, however, the impact on NADPH becomes particularly relevant at strongly oxidized NADH levels (Figure 4F). Together, these data imply that acceleration of NADH-coupled respiration during metabolic perturbations facilitates Nnt-mediated NADPH oxidation, while Nnt-deficiency maintains the NADPH pool under these conditions.

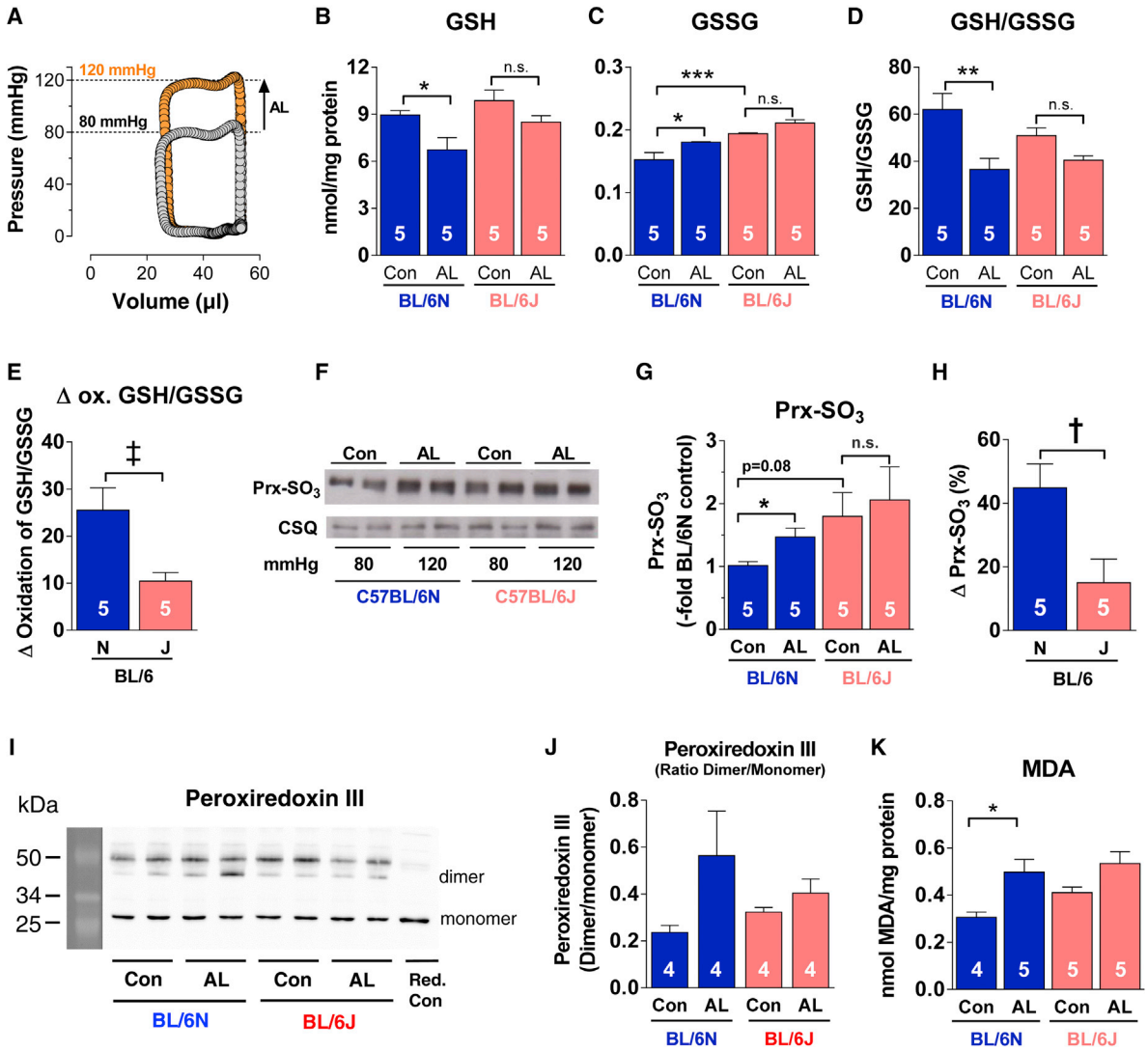

Figure 5. Increasing Afterload Induces Nnt-Mediated Oxidation of Glutathione and Peroxiredoxin

Isolated working hearts from BL/6N and BL/6J mice were held at a preload of 10 mmHg and afterload of 80 mmHg (400 bpm). Afterload was increased to 120 mmHg (AL) or maintained at 80 mmHg (Con). After 15 min, hearts were snap-frozen for biochemical analyses.

(A–D) Representative pressure-volume loops (A), concentration of reduced glutathione (GSH) (B) and oxidized glutathione (GSSG) (C), and ratio of GSH/GSSG (D), respectively (n = 5 per group).

(E) Degree of oxidation of GSH/GSSG by AL in BL/6N and BL/6J hearts.

(F) Representative western blot determining expression of oxidized peroxiredoxin (Prx-SO_3) and calsequestrin (CSQ) in BL/6N and BL/6J hearts, respectively.

(G) Quantification of Prx-SO_3 relative to CSQ expression and normalized to Con in BL/6N hearts.

(H) Relative increase of Prx-SO_3 in response to AL (fold change of BL/6N Con).

(I) Western -blot analysis of monomeric and dimeric peroxiredoxin III. Red. Con, reduced Control.

(J) Quantification of dimeric/monomeric peroxiredoxin III.

(K) Quantification of malondialdehyde (MDA) concentrations.

Data are presented as means ± SEM. *p < 0.05, **p < 0.01, and ***p < 0.001 (ANOVA, Tukey's post test); †p < 0.05, ‡p < 0.01 (unpaired t test; all groups n = 5).

Reverse-Mode Nnt Oxidizes Glutathione and Peroxiredoxin in Response to Increased Afterload

To test the relevance of reverse-mode Nnt on the whole organ level, we performed experiments on isolated working hearts exposed to a physiological pre- and afterload of 10 and 80 mmHg, respectively. Under these conditions, the redox states of glutathione and peroxiredoxin, which are regenerated by NADPH (Figure 1A), were slightly more oxidized in BL/6J versus BL/6N hearts (Figures 5C, 5D, 5F, and 5G). In contrast, when afterload was increased from 80 to 120 mmHg for 15 min (Figure 5A), it led to stronger oxidation of glutathione and peroxiredoxin in BL/6N versus BL/6J hearts (Figures 5B–5H). Reduced peroxiredoxin exists in a monomeric form, while oxidation causes dimerization (Kumar et al.,

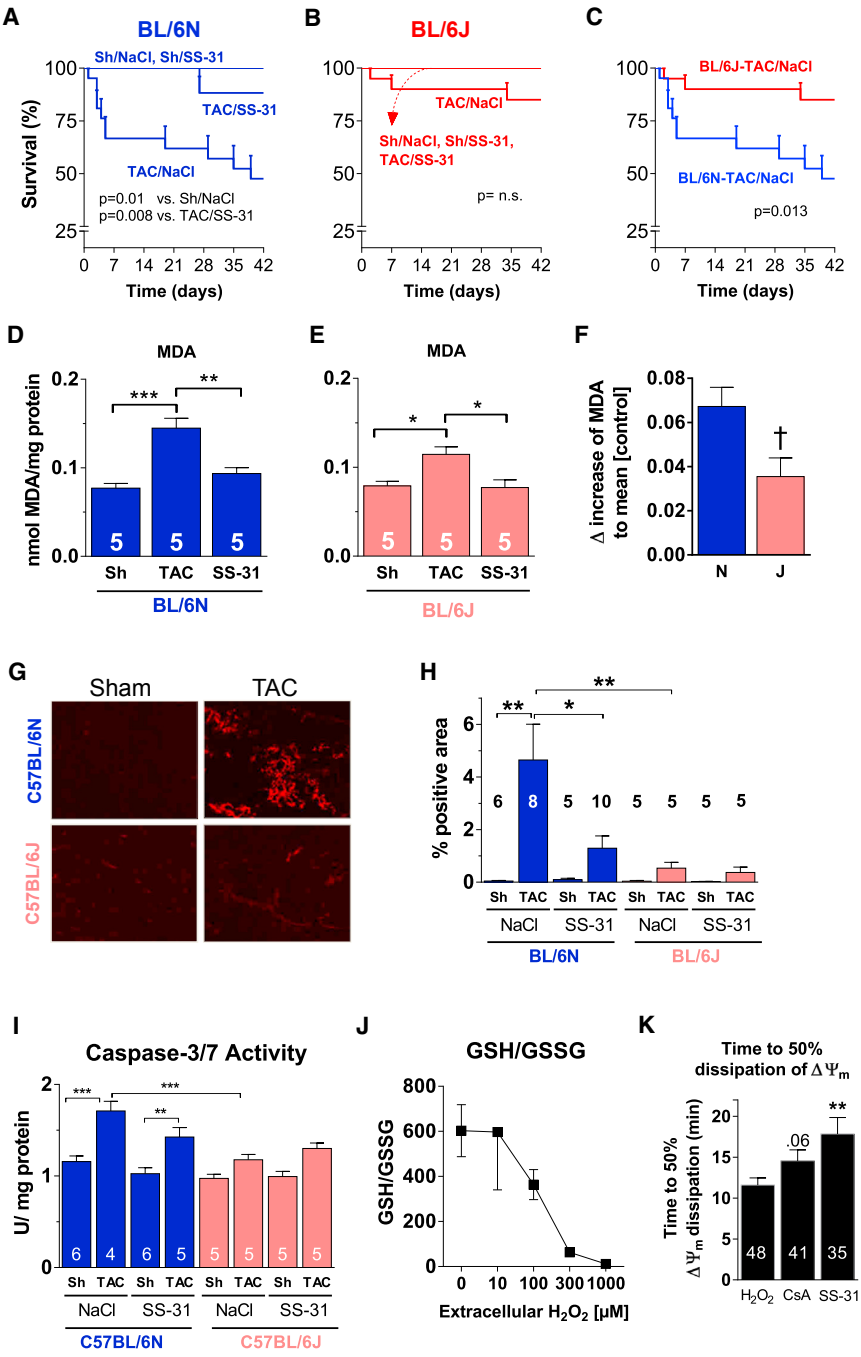

Figure 6. Decreased Mortality and Necrosis in BL/6J Mice after Pressure Overload

BL/6N and BL/6J mice were exposed to a combined operation of TAC or sham plus implantation of a minipump releasing SS-31 (3 mg/kg per day) or vehicle (NaCl 0.9%) for 6 weeks (A–F) or 3 days (G–I), respectively.

(A) Kaplan-Meier survival curves in Sham- or TAC-treated BL/6N mice, treated with SS-31 or vehicle, respectively.

(B) Kaplan-Meier survival of same groups as in (A), but in BL/6J mice.

(C) Comparison of Kaplan-Meier survival curves in TAC/vehicle-treated BL/6N and BL/6J mice.

(D) MDA concentrations in Sham- or TAC-treated BL/6N mice, the latter treated with vehicle or SS-31.

(E) Same as in (D), but in BL/6J mice.

(F) Comparison of the absolute increase in MDA in BL/6N (N) and BL/6J mice (J).

(G) Histological analyses of Evans blue staining in Sham- and TAC-treated BL/6N and BL/6J mice (vehicle groups), respectively.

(H) Quantification of Evans Blue staining. Sh, Sham.

(I) Caspase-3 and caspase-7 activities in the same groups as in (H).

(J) GSH/GSSG in isolated Langendorff-perfused BL/6N hearts exposed to H_2O_2.

(K) Time to 50% dissipation of $\Delta\Psi_m$ (TMRM) in isolated BL/6N cardiac myocytes exposed to 100 μmol/l H_2O_2, in the absence (H_2O_2) and presence of cyclosporine A (CsA; 10 μM) or SS-31 (10 nM), respectively.

Data are presented as means ± SEM. *$p < 0.05$, **$p < 0.01$, and ***$p < 0.001$ (one-way ANOVA, Tukey's post test). †$p < 0.05$ (unpaired t test). See also Figure S4.

Targeting Mitochondrial ROS Production Reduces Necrosis and Early Mortality in Response to Increased Afterload In Vivo

To analyze whether mitochondrial ROS production is the key difference between BL/6N and BL/6J mice in response to increased afterload, we combined TAC or sham-operation with the implantation of osmotic minipumps releasing either vehicle or SS-31, a tetrapeptide that reduces mitochondrial ROS production (Szeto, 2014). Vehicle-treated BL/6N mice suffered ~50% mortality in 6 weeks, while most BL/6J mice survived this intervention (Figures 6A–6C). SS-31 reduced TAC-induced mortality in BL/6N mice to levels of vehicle-treated BL/6J mice (Figures 6A and 6B). Although TAC-induced increases in lipid peroxidation were more pronounced in BL/6N than in BL/6J mice and sensitive to SS-31 (Figures 6D–6F), no differences in cardiac hypertrophy were observed between strains and by treatment (Figures S4A and S4B). Despite a mortality-induced selection bias, SS-31 ameliorated *ANP* upregulation in BL/6N mice, while the TAC-induced increase in *CTGF* was insensitive to SS-31 (Figures S4C and S4D).

2009). Upon afterload elevation, the degree of dimerization of the mitochondrial isoform peroxiredoxin III was increased in BL/6N, but not BL/6J hearts (Figures 5I and 5J), further pinpointing mitochondria as the main source for oxidative stress under these conditions. Accordingly, afterload-induced increases in lipid peroxidation were more pronounced in BL/6N than in BL/6J hearts (Figure 5K). Taken together, these data are in good agreement with the in vivo data (Figures 2H and 2I), where ROS levels were slightly lower in sham-operated-, but much higher in TAC-operated BL/6N versus BL/6J mice.

Mitochondrial ROS can trigger the opening of the permeability transition pore (PTP), dissipate $\Delta\Psi_m$, and induce apoptotic and/or necrotic cell death (Halestrap, 2005). After only 3 days of TAC, necrotic cell death increased in hearts of TAC-operated BL/6N, but not BL/6J mice (Figure 6G). For any given increase in *ANP* expression as an index of hemodynamic load, TAC-induced necrosis was 4- to 5-fold more pronounced in BL/6N mice than in BL/6J mice (not shown), and this was prevented by SS-31 (Figure 6H). Similar, albeit less pronounced results were obtained for the activities of caspase-3 and caspase-7 as inducers of apoptosis (Figure 6I). The PTP inhibitor cyclosporin A reduced necrosis in TAC-treated BL/6N hearts (to 1.3% ± 0.4%). However, due to a slight anti-necrotic effect of the oil-based vehicle, this effect was not significantly different from its control (not shown). Further experiments on isolated mitochondria revealed that ameliorated necrosis in BL/6J mice was not related to modified properties of the PTP per se, since Ca^{2+} and ROS induced similar PTP opening in both strains (Figures S4E and S4F).

To test whether the levels of oxidative stress that occur after TAC in BL/6N mice are sufficient to induce cardiomyocyte death, we exposed isolated perfused BL/6N hearts to increasing concentrations of exogenous H_2O_2 and observed that 100 μM H_2O_2 oxidized the glutathione pool by 40% (Figure 6J), a similar extent as after increasing afterload from 80 to 120 mmHg in working hearts (41%; Figure 5D). Applying 100 μM H_2O_2 to isolated BL/6N cardiomyocytes dissipated $\Delta\Psi_m$ by 50% after ~12 min, which was delayed by cyclosporin A and even more by SS-31 (Figure 6K).

Re-expression of the Nnt in BL/6J Mice Re-establishes Oxidative Stress in Response to Pressure Overload

To rule out that other genomic differences between BL/6N and BL/6J mice (Simon et al., 2013) account for differential ROS production, we obtained BL/6J mice that harbor one allele with the intact wild-type (*wt*) and one with the truncated (*t*) *Nnt* gene (BL/6J-$Nnt^{wt/t}$) (Kim et al., 2010). From this strain, we generated BL/6J-$Nnt^{t/t}$, BL/6J-$Nnt^{wt/t}$, and BL/6J-$Nnt^{wt/wt}$ mice. Re-expression of intact *Nnt* in BL/6J mice increased Nnt activity to levels observed in BL/6N mice (Figure 7A). Three days after TAC, mRNA expression of brain natriuretic peptide (*BNP*), an index of LV filling pressures, increased (Figure 7B), together with more pronounced oxidation of peroxiredoxin and oxidative stress (indexed by 8-OHdG) in wild-type *Nnt*-expressing mice in vivo (Figures 7C–7F). For any given TAC-induced increase of cardiomyocyte cross sectional area, the increase in ROS in vivo was higher in BL/6J-$Nnt^{wt/wt}$ mice compared to BL/6J-$Nnt^{t/t}$ or BL/6J-$Nnt^{wt/t}$ (Figure 7G). Taken together, these data indicate that the lower TAC-induced mitochondrial ROS emission in BL/6J mice was primarily related to the absence of a functional Nnt.

DISCUSSION

Our study revealed that besides its canonical antioxidant function, the mitochondrial transhydrogenase (Nnt) can switch to a pro-oxidative reverse mode that triggers NADPH oxidation during a pathological increase of workload in cardiac mitochondria (Figure 7H). This pro-oxidative shift provokes mitochondrial ROS emission and induces necrotic cell death, fibrosis, cardiac dysfunction, and death. To our knowledge, this is the first bona fide mechanism that explains how a pathological increase in cardiac workload per se increases mitochondrial ROS emission independent of neuroendocrine activation. The missense of a functional Nnt in BL/6J mice substantially ameliorates oxidative stress, maladaptive remodeling, and LV dysfunction and reduces death in response to pressure overload. This finding has broad implications since it sheds new light on many previous studies using this strain to analyze the consequences of other, non-mitochondrial sources of ROS for cardiac remodeling and the development of heart failure. Furthermore, differential tissue-specific expression of the Nnt adds another level of complexity to the regulation of mitochondrial ROS emission in different tissues under variable metabolic conditions. Finally, targeting mitochondrial ROS production with the tetrapeptide SS-31, which is already in clinical testing, may be an efficient therapy of heart failure.

Pathophysiological Role of Mitochondrial ROS in Heart Failure

Oxidative stress in the plasma and myocardium of patients with heart failure correlates with LV dysfunction (Belch et al., 1991; Maack et al., 2003). Besides mitochondria, other relevant ROS sources in cardiac myocytes are NADPH oxidases, uncoupled nitric oxide synthases, monoamine oxidase A, and xanthine oxidase. The relative contribution of these sources to overall myocardial ROS production during the development of heart failure, however, is unknown. A common approach to estimate the role of a particular ROS source is to apply TAC in mice with genetic modifications of proteins involved in ROS production. In fact, most of these studies were performed on BL/6J mice (Table S1). Our data indicate that in BL/6J mice, contribution of mitochondria to cellular ROS production, and maladaptive remodeling in response to TAC is heavily underestimated or even absent (Figure 2I), implying that studies using BL/6J may overestimate the contribution of non-mitochondrial ROS sources. In contrast, overexpressing a mitochondria-targeted catalase in BL/6N mice protected hearts from maladaptive remodeling in response to TAC (Dai et al., 2012). Since in our study, inhibiting mitochondrial ROS emission with the tetrapeptide SS-31 rescued TAC-induced mortality in BL/6N, but not BL/6J mice, these data imply that mitochondria are the dominant source of ROS during pathological elevations of afterload. In humans, chronic elevations of afterload are a central feature of various cardiovascular diseases, such as arterial hypertension, aortic stenosis or vascular stiffness imposed by atherosclerosis and/or aging. All these age-associated conditions are known risk factors for the development of heart failure. A previous study observed downregulation of Nnt activity in human failing hearts, which was associated with oxidation of glutathione (Sheeran et al., 2010). While these authors suggested that downregulation of Nnt activity may contribute to oxidative stress, the data of our study rather imply that Nnt downregulation in human heart failure may be protective by reducing reverse-mode Nnt-mediated mitochondrial ROS emission.

Already 3 days after TAC, the rates of apoptosis and necrosis were strikingly different between strains. In human heart failure, the levels of apoptosis are increased (Olivetti et al., 1997), and even low rates of cardiomyocyte death are sufficient to cause a lethal dilated cardiomyopathy (Wencker et al., 2003). In human

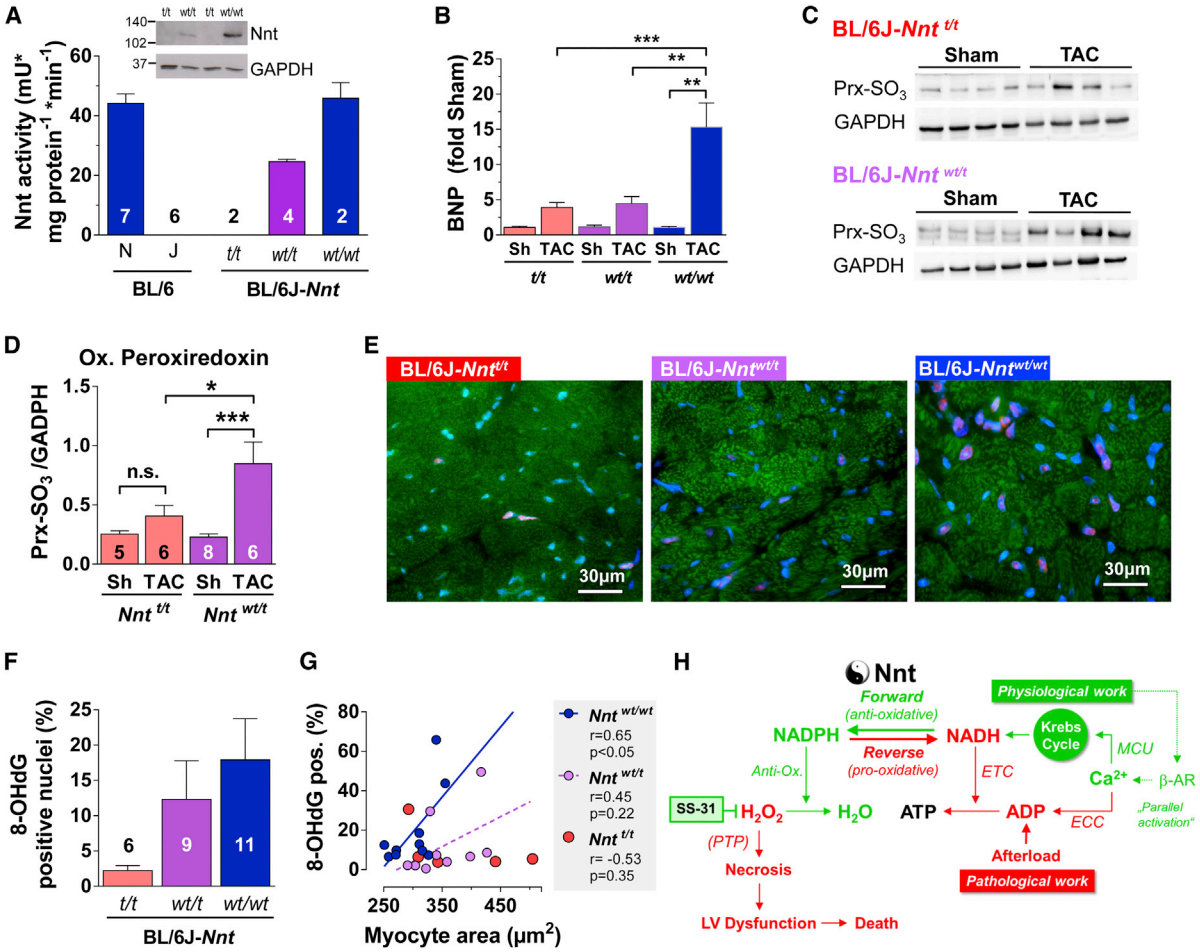

Figure 7. Re-expression of Nnt in BL/6J Mice Increases Oxidative Stress In Vivo

(A) Nnt activity in BL/6N and BL/6J mice, compared with N5 BL/6J-*Nnt*$^{t/t}$ mice (with two alleles of the truncated (*t*) *Nnt* gene) and mice with heterozygous (BL/6J-*Nnt*$^{wt/t}$) and homozygous re-expression of the wild-type Nnt gene (BL/6J-*Nnt*$^{wt/wt}$). Inset: western blot analysis of Nnt and GAPDH in mouse LV as indicated.

(B) mRNA expression of BNP in LV of BL/6J-*Nnt*$^{t/t}$, BL/6J-*Nnt*$^{wt/t}$ and BL/6J-*Nnt*$^{wt/wt}$ mice after sham or TAC surgery, respectively.

(C) Western blot analysis of oxidized peroxiredoxin (Prx-SO_3) and GAPDH in LV of BL/6J-*Nnt*$^{t/t}$ and BL/6J-*Nnt*$^{wt/t}$ mice after sham or TAC surgery, respectively.

(D) Quantification of data in (C).

(E) Representative histographs of 8-OHdG staining in LV of BL/6J-*Nnt*$^{t/t}$, BL/6J-*Nnt*$^{wt/t}$, and BL/6J-*Nnt*$^{wt/wt}$ mice after TAC, respectively.

(F) Quantification of data in (E).

(G) Plotting of 8-OHdG staining against myocyte cross sectional area in BL/6J-*Nnt*$^{t/t}$, BL/6J-*Nnt*$^{wt/t}$, and BL/6J-*Nnt*$^{wt/wt}$ mice after TAC, respectively.

(H) Scheme of proposed mode of action of Nnt during physiological and pathological cardiac workloads.

Data are presented as means ± SEM. *p < 0.05, **p < 0.01, and ***p < 0.001 (ANOVA, Tukey's post test).

heart failure, elevated levels of high-sensitive troponin T, a marker for cardiomyocyte necrosis, predict an adverse clinical outcome (Masson et al., 2012). SS-31 accumulates in mitochondria and protects cardiolipin and other mitochondrial proteins from oxidative damage, which may interrupt a feed-forward pathway of mitochondrial dysfunction and ROS production (Dai et al., 2013; Szeto, 2014). In our study, SS-31 prevented necrosis and (partly) apoptosis, while *CTGF* upregulation appeared unaffected. These data are in agreement with, and at the same time extend, previous data in which SS-31 prevented 84% of TAC-induced proteomic remodeling in BL/6N mitochondria (Dai et al., 2013). Ongoing clinical studies will have to verify whether SS-31 is of clinical use in patients with heart failure (Szeto, 2014).

Reverse-Mode Nnt Modifies Current Paradigm of Mitochondrial ROS Production

The current paradigm of mitochondrial ROS production implies that dissipating $\Delta\Psi_m$ by accelerating respiration with ADP (or activation of uncoupling proteins) generally reduces mitochondrial oxidative stress (Balaban et al., 2005). In contrast, we observed that H_2O_2 emission was lowered by ADP only in the absence of an Nnt in BL/6J, but not BL/6N cardiac mitochondria. This is in seeming contrast to other studies on which the current paradigm is based on. For instance, in isolated rat cardiac mitochondria, H_2O_2 emission decreased when respiration was accelerated by ADP or chemical uncoupling (Korshunov et al., 1997). In that study, however, the mitochondrial H_2O_2-scavenging capacity

was eliminated by pretreatment of mitochondria with H_2O_2 and aminotriazole, so that H_2O_2 emission was governed primarily by $^{\bullet}O_2^-$ production at the ETC and no longer counterbalanced by NADPH-dependent H_2O_2 elimination. Furthermore, H_2O_2 emission from brain mitochondria was maximal at reduced redox states of NAD(P)H, while chemical or ADP-induced uncoupling of $\Delta\Psi_m$ lowered it (Starkov and Fiskum, 2003). However, brain mitochondria do not express the Nnt (Figure S1B), and we could reconcile their findings in brain mitochondria from BL/6N mice, where ADP reduced H_2O_2 emission to a similar extent as in brain mitochondria from BL/6J mice (Figure S3). Taken together, differential Nnt expression accounts for tissue-specific differences in the regulation of mitochondrial ROS emission that may also explain why in contrast to results on brain mitochondria (Starkov and Fiskum, 2003), we previously observed an inverse (and not positive) correlation between the redox state of NAD(P)H and H_2O_2 emission in cardiac myocytes (Kohlhaas et al., 2010).

Organ-Specific Relevance of Nnt for Antioxidative Capacity

Interestingly, under physiological (unstressed) conditions, impaired glucose tolerance due to ROS-dependent impairment of insulin release is so far the only known phenotype provoked by the mutation of the *Nnt* in BL/6J mice (Simon et al., 2013; Toye et al., 2005). One explanation may be that the high efficacy of IDH2 to regenerate NADPH (Figures S1F and S1H) can compensate for the loss of the Nnt at least in cardiac mitochondria. In contrast, in pancreatic islets from BL/6N and BL/6J mice we observed that in the presence of physiological levels of ATP, IDH2 activity was largely suppressed (Figures S1I and S1J). Thus, when high glucose triggers an elevation of ATP and insulin secretion in the pancreas, the lack of Nnt in BL/6J may deteriorate the NADPH regenerative capacity and induce oxidative stress to a higher extent in this organ compared to other organs in which IDH2 can compensate for the loss of Nnt.

Limitations

Since we did not apply knockout technology, we cannot fully rule out that apart from Nnt expression, also other genetic differences between BL/6N and BL/6J mice may contribute to the differences in oxidative stress and/or maladaptive remodeling between the strains. However, since (1) re-expression of one or two wild-type *Nnt* alleles in BL/6J mice re-increased oxidative stress after TAC (Figure 7), and (2) no differences in mitochondrial $^{\bullet}O_2^-$ production or H_2O_2 emission were observed between the strains in the absence of ADP (State 4; Figures 3B and 3C), other mechanisms than differential Nnt expression appear unlikely to account for the differences in ROS emission when ADP accelerates respiration at higher workloads. Another limitation is that NADPH could not be measured directly and separated from fluorescent NADH signals, which is technically challenging. Nevertheless, the information gathered from NADPH/NADH ratios determined by FLIM (Figures 3J and 3K) during mitochondrial perturbations and data from computational modeling (Figure 4) support the concept that oxidation of NADH at the ETC can provoke the reverse mode of the Nnt to oxidize NADPH.

Conclusions

We identified a mechanism that couples a pathological increase in metabolic demand to increased mitochondrial ROS emission in the heart (Figure 7H). The discovery of the previously unappreciated reverse-mode of the Nnt assigns this enzyme a dual role serving either pro- or antioxidative processes depending on the metabolic state of a cell. Considering the overarching importance of ROS production in aging and aging-related diseases, these data provide important new insights into the mechanisms of redox regulation under physiological and pathological conditions in various tissues. Targeting mitochondrial ROS emission is therefore a promising approach to ameliorate aging-related diseases and in particular, heart failure.

EXPERIMENTAL PROCEDURES

Animal Experiments

Animal procedures were approved by the local animal ethics committee and conducted in accordance with institutional guidelines. C57BL/6 mice were obtained from Charles River (BL/6N, C57BL/6NCrl, strain code 027; and BL/J, C57BL/6J, JAX Mice Stock Number 000664). N5 BL/6J-*Nnt*$^{wt/t}$ mice (Kim et al., 2010) were obtained from Jackson Laboratories and further bred at our institution, generating BL/6J-*Nnt*$^{t/t}$, BL/6J-*Nnt*$^{wt/t}$ and BL/6J-*Nnt*$^{wt/wt}$ mice.

Transaortic Constriction

Transaortic constriction (TAC) was performed as described in more detail in the Supplemental Experimental Procedures. Mice (10- to 12-week-old) underwent TAC or sham surgery and were followed for 6 weeks or 3 days. A literature research was performed for other studies that performed TAC in normal or genetically modified BL/6N and BL/6J mice (Table S1). For drug treatment, osmotic minipumps (Alzet #2006) were implanted ~20 min after TAC and loaded with SS-31 (3 mg/kg × d) or vehicle (0.9% NaCl) for 6 weeks. In 3-day experiments, SS-31 was injected intraperitoneally (i.p.) (0.5 mg/ml, 0.9% NaCl) and compared to 0.9% NaCl.

Echocardiography

Echocardiography was performed as described in more detail in the Supplemental Experimental Procedures section on anaesthetized mice using a Visualsonics Vevo 770 High-Resolution in vivo Micro-Imaging System (Visualsonics).

Isolated Working Hearts Experiments

For hemodynamics, hearts were mounted in a working heart apparatus and analyzed with a pressure-volume catheter as described in the Supplemental Experimental Procedures. Hearts equilibrated at 10 mmHg preload and 80 mmHg afterload at 400 bpm external pacing. Then afterload was increased to 120 mmHg or maintained at 80 mmHg for 15 min.

Isolated Cardiac Myocytes

Cardiac myocytes were isolated by enzymatic digestion and experiments performed as described in the Supplemental Experimental Procedures and Table S2. Briefly, adult ventricular myocytes were electrically stimulated at 0.5 Hz and then exposed to isoproterenol (30 nM) and an increase of stimulation rate to 5 Hz for 3 min. Sarcomere shortening was detected together with either (1) the redox state of NAD(P)H/NAD(P)$^+$ and $FADH_2$/FAD by autofluorescence, (2) $\Delta\Psi_m$ (with tetramethylrhodamine methyl ester; TMRM) together with $[Ca^{2+}]_c$ (indo-1 acetoxymethyl esther; AM), (3) mitochondrial $^{\bullet}O_2^-$ formation (MitoSOX), or (4) cellular H_2O_2 formation (using 5-(-6)-chloromethyl-2,7-dichlorohydrofluorescein di-acetate; CM-H_2DCFDA). Using a patch-clamp-based protocol with application of indo-1 salt and rhod-2 AM, $[Ca^{2+}]_c$ was determined together with $[Ca^{2+}]_m$ under similar conditions (Maack et al., 2006).

Quiescent myocytes (Figures 3F and 3G) were exposed to FCCP (5 μM), cyanide (4 mM), and H_2O_2 (10 mM) and NAD(P)H/NAD(P)$^+$ and $FADH_2$/FAD were determined in the same cells, respectively. $\Delta\Psi_m$ (TMRM) was determined together with NAD(P)H in myocytes exposed to FCCP (5 μM) and oligomycin (1.26 μM; Figures S3G–S3J).

NAD(P)H Fluorescence Lifetime Imaging Experiments

Cardiac myocytes were allowed to adhere to glass coverslips for >2 hr before imaging. At the microscope, coverslips were maintained at 37°C in a home built chamber and bathed in DMEM (GIBCO) containing (in mM) glucose 25, pyruvate 1, glutamine 2, and HEPES 10. NAD(P)H fluorescence lifetime imaging (FLIM) was described previously (Blacker et al., 2014) and in further detail in the Supplemental Experimental Procedures. Five minutes prior to application of pharmacological treatments, 10 μM blebbistatin was applied to prevent contraction during FLIM image acquisition. Control experiments showed that blebbistatin did not alter the FLIM parameters α_{bound} ($p = 0.2$, $n = 3$, 14 images), τ_{free} ($p = 0.2$) or τ_{bound} ($p = 0.1$).

Isolated Mitochondria

Mitochondria were isolated from heart, brain and skeletal muscle by standard techniques as described in the Supplemental Experimental Procedures. Mitochondria were supplied with pyruvate/malate as substrates (5/5 mM). Respiration (Clark electrode), $\bullet O_2^-$ formation (electron paramagnetic resonance, EPR), H_2O_2 emission (Amplex Ultra-Red), or NAD(P)H autofluorescence were determined in the absence or presence of ADP (1 mM), respectively. $\Delta\Psi_m$ was determined using triphenylmethylphosphonium ($TPMP^+$).

Real-Time PCR, Gene Array, and Western Blot Analysis

Real-time PCR, gene array, and western blot analyses were performed by standard techniques as described in more details in the Supplemental Experimental Procedures. The secondary antibody against Nnt was provided by Ting-Ting Huang (University of California, San Francisco). Gene array experiments were performed using the Affymetrix GeneChip Mouse Gene 1.0 ST Array. The gene array accession number of the data in Tables S3 and S4 is "E-MTAB-2732" at ArrayExpress.

Histological Analyses

Histological analyses were performed by standard techniques with details outlined in the Supplemental Experimental Procedures. H&E staining was used for cardiomyocyte morphometry, picrosirius red staining for fibrosis, and 8-hydroxy-2′-deoxyguanosine (8-OHdG) for intracellular ROS detection. Evans blue staining (indexing necrosis) was detected after i.p. application of 100 μl of Evans blue solution (16.7 mg/ml) 1 day before sacrifice.

Enzyme Activities

Details on enzymatic activity measurements are provided in the Supplemental Experimental Procedures. Activities of Nnt, IDH2, and MEP were analyzed by NADPH- or APAD-coupled spectrophotometric assays in homogenates of isolated cardiac mitochondria.

GSH/GSSG Measurements

Determination of GSH and GSSG was performed as described previously (Rahman et al., 2006) and as outlined in more detail in the Supplemental Experimental Procedures. For GSSG measurements, 3 mM of 1-methyl-2-vinylpyridine was added for derivatization of reduced GSH before homogenization. Reduced GSH was calculated as the difference between total glutathione and GSSG.

Malondialdehyde Concentrations

Lipid peroxidation was determined using the ALDetect Lipid Peroxidation Assay Kit (ENZO Life Science) to detect the concentrations of malondialdehydes (MDA) according to the manufacturer's protocol. As a variation from that protocol, the sample volume was reduced from 200 μl to 150 μl.

Caspase-3/7 Activity

The Caspase-Glo 3/7 Assay (Promega) was used to measure caspase-3 and caspase-7 activities. Heart lysates (50 μg) were mixed with reaction solution at equal volumes in a 96-well plate. Luminescence was detected after 20 min (at 37°C) and activities normalized to a standard of caspase-3.

Computational Modeling

Computational modeling of NADH, NADPH, $\Delta\Psi_m$, and Nnt activity was performed with the integrated model of mitochondrial energetics, redox, and ROS metabolic networks (Kembro et al., 2013). The model parameters were as in Kembro et al. (2013), except for cytoplasmic ADP that was driven by an exogenous function. The baseline level of cytoplasmic ADP was 5 μM, with pulses of 20, 30, and 40 μM added for 200 s as shown by the ADP_m transients in Figure 4A. To simulate the absence of Nnt activity, its forward and reverse rate constants were reduced 10,000-fold.

Statistical Analyses

Values are displayed as mean ± SEM. One-way ANOVA followed by Tukey's multiple comparisons test, paired, and unpaired t tests, Fisher's exact test, and Kaplan-Meier survival analyses were performed using GraphPad Prism version 6.00 for Windows (GraphPad, http://www.graphpad.com).

ACCESSION NUMBERS

The accession number for the gene array reported in this paper is ArrayExpress E-MTAB-2732.

SUPPLEMENTAL INFORMATION

Supplemental Information includes Supplemental Experimental Procedures, four figures, and four tables and can be found with this article online at http://dx.doi.org/10.1016/j.cmet.2015.07.008.

AUTHOR CONTRIBUTIONS

C.M. and A.G.N. designed the study and wrote the manuscript. A.G.N., A.v.H., M. Hohl, J.R.L., J.B, J.-C.R., A.K., J.B., M.S., S.-L.P., M.K., M.W., I.B., B.P., M.L., T.S.B., A.R.H., L.K., T.Z., S.C., C. Müller, and A.K. performed the experiments. C.R.D.L., I.B., R.K., M. Hoth, M.R.D., U.L., M.B., P.L., and S.C. gave valuable scientific input and supervised data analysis and experiments.

ACKNOWLEDGMENTS

The study was supported by the Deutsche Forschungsgemeinschaft (Emmy Noether- and Heisenberg Programm to C. Maack; SFB 894 to M. Hoth and C. Maack; KFO 196 to C. Maack, U.L, A.K., M.B.; and SFB 1027 to M. Hoth (project A2) and I.B. (project C4); BO3643/3-1 to I.B.), the Deutsche Gesellschaft für Kardiologie (Otto Hess Stipendium to M.S.) and the Staatskanzlei Saarland (LFFP 11/02 and 15/04) (to C.R.D.L.). U.L. and C. Maack are supported by the Corona foundation. We thank Michelle Gulentz, Lisa Lang, Jeanette Zimolong, and Nina Schnellbach for technical assistance and Ting-Ting Huang (Stanford University, CA) for providing the antibody against Nnt.

Received: January 26, 2015
Revised: May 10, 2015
Accepted: July 8, 2015
Published: August 6, 2015

REFERENCES

Ago, T., Liu, T., Zhai, P., Chen, W., Li, H., Molkentin, J.D., Vatner, S.F., and Sadoshima, J. (2008). A redox-dependent pathway for regulating class II HDACs and cardiac hypertrophy. Cell *133*, 978–993.

Aon, M.A., Cortassa, S., and O'Rourke, B. (2010). Redox-optimized ROS balance: a unifying hypothesis. Biochim. Biophys. Acta *1797*, 865–877.

Backx, P.H., and Ter Keurs, H.E. (1993). Fluorescent properties of rat cardiac trabeculae microinjected with fura-2 salt. Am. J. Physiol. *264*, H1098–H1110.

Balaban, R.S. (2002). Cardiac energy metabolism homeostasis: role of cytosolic calcium. J. Mol. Cell. Cardiol. *34*, 1259–1271.

Balaban, R.S., Nemoto, S., and Finkel, T. (2005). Mitochondria, oxidants, and aging. Cell *120*, 483–495.

Belch, J.J., Bridges, A.B., Scott, N., and Chopra, M. (1991). Oxygen free radicals and congestive heart failure. Br. Heart J. *65*, 245–248.

Blacker, T.S., Mann, Z.F., Gale, J.E., Ziegler, M., Bain, A.J., Szabadkai, G., and Duchen, M.R. (2014). Separating NADH and NADPH fluorescence in live cells and tissues using FLIM. Nat. Commun. *5*, 3936.

Brandes, R., and Bers, D.M. (1997). Intracellular Ca^{2+} increases the mitochondrial NADH concentration during elevated work in intact cardiac muscle. Circ. Res. *80*, 82–87.

Cortassa, S., Aon, M.A., O'Rourke, B., Jacques, R., Tseng, H.J., Marbán, E., and Winslow, R.L. (2006). A computational model integrating electrophysiology, contraction, and mitochondrial bioenergetics in the ventricular myocyte. Biophys. J. *91*, 1564–1589.

Dai, D.F., Santana, L.F., Vermulst, M., Tomazela, D.M., Emond, M.J., MacCoss, M.J., Gollahon, K., Martin, G.M., Loeb, L.A., Ladiges, W.C., and Rabinovitch, P.S. (2009). Overexpression of catalase targeted to mitochondria attenuates murine cardiac aging. Circulation *119*, 2789–2797.

Dai, D.F., Hsieh, E.J., Liu, Y., Chen, T., Beyer, R.P., Chin, M.T., MacCoss, M.J., and Rabinovitch, P.S. (2012). Mitochondrial proteome remodelling in pressure overload-induced heart failure: the role of mitochondrial oxidative stress. Cardiovasc. Res. *93*, 79–88.

Dai, D.F., Hsieh, E.J., Chen, T., Menendez, L.G., Basisty, N.B., Tsai, L., Beyer, R.P., Crispin, D.A., Shulman, N.J., Szeto, H.H., et al. (2013). Global proteomics and pathway analysis of pressure-overload-induced heart failure and its attenuation by mitochondrial-targeted peptides. Circ Heart Fail *6*, 1067–1076.

Freeman, H., Shimomura, K., Horner, E., Cox, R.D., and Ashcroft, F.M. (2006). Nicotinamide nucleotide transhydrogenase: a key role in insulin secretion. Cell Metab. *3*, 35–45.

Halestrap, A. (2005). Biochemistry: a pore way to die. Nature *434*, 578–579.

Huang, T.T., Naeemuddin, M., Elchuri, S., Yamaguchi, M., Kozy, H.M., Carlson, E.J., and Epstein, C.J. (2006). Genetic modifiers of the phenotype of mice deficient in mitochondrial superoxide dismutase. Hum. Mol. Genet. *15*, 1187–1194.

Kembro, J.M., Aon, M.A., Winslow, R.L., O'Rourke, B., and Cortassa, S. (2013). Integrating mitochondrial energetics, redox and ROS metabolic networks: a two-compartment model. Biophys. J. *104*, 332–343.

Kim, A., Chen, C.H., Ursell, P., and Huang, T.T. (2010). Genetic modifier of mitochondrial superoxide dismutase-deficient mice delays heart failure and prolongs survival. Mamm. Genome *21*, 534–542.

Kohlhaas, M., Liu, T., Knopp, A., Zeller, T., Ong, M.F., Böhm, M., O'Rourke, B., and Maack, C. (2010). Elevated cytosolic Na^+ increases mitochondrial formation of reactive oxygen species in failing cardiac myocytes. Circulation *121*, 1606–1613.

Korshunov, S.S., Skulachev, V.P., and Starkov, A.A. (1997). High protonic potential actuates a mechanism of production of reactive oxygen species in mitochondria. FEBS Lett. *416*, 15–18.

Kumar, V., Kitaeff, N., Hampton, M.B., Cannell, M.B., and Winterbourn, C.C. (2009). Reversible oxidation of mitochondrial peroxiredoxin 3 in mouse heart subjected to ischemia and reperfusion. FEBS Lett. *583*, 997–1000.

Lee, H.Y., Choi, C.S., Birkenfeld, A.L., Alves, T.C., Jornayvaz, F.R., Jurczak, M.J., Zhang, D., Woo, D.K., Shadel, G.S., Ladiges, W., et al. (2010). Targeted expression of catalase to mitochondria prevents age-associated reductions in mitochondrial function and insulin resistance. Cell Metab. *12*, 668–674.

Lin, M.T., and Beal, M.F. (2006). Mitochondrial dysfunction and oxidative stress in neurodegenerative diseases. Nature *443*, 787–795.

Maack, C., Kartes, T., Kilter, H., Schäfers, H.J., Nickenig, G., Böhm, M., and Laufs, U. (2003). Oxygen free radical release in human failing myocardium is associated with increased activity of rac1-GTPase and represents a target for statin treatment. Circulation *108*, 1567–1574.

Maack, C., Cortassa, S., Aon, M.A., Ganesan, A.N., Liu, T., and O'Rourke, B. (2006). Elevated cytosolic Na^+ decreases mitochondrial Ca^{2+} uptake during excitation-contraction coupling and impairs energetic adaptation in cardiac myocytes. Circ. Res. *99*, 172–182.

Masson, S., Anand, I., Favero, C., Barlera, S., Vago, T., Bertocchi, F., Maggioni, A.P., Tavazzi, L., Tognoni, G., Cohn, J.N., et al. (2012). Serial measurement of cardiac troponin T using a highly sensitive assay in patients with chronic heart failure: data from 2 large randomized clinical trials. Circulation *125*, 280–288.

Matsushima, S., Ide, T., Yamato, M., Matsusaka, H., Hattori, F., Ikeuchi, M., Kubota, T., Sunagawa, K., Hasegawa, Y., Kurihara, T., et al. (2006). Overexpression of mitochondrial peroxiredoxin-3 prevents left ventricular remodeling and failure after myocardial infarction in mice. Circulation *113*, 1779–1786.

Murphy, M.P. (2009). How mitochondria produce reactive oxygen species. Biochem. J. *417*, 1–13.

Olivetti, G., Abbi, R., Quaini, F., Kajstura, J., Cheng, W., Nitahara, J.A., Quaini, E., Di Loreto, C., Beltrami, C.A., Krajewski, S., et al. (1997). Apoptosis in the failing human heart. N. Engl. J. Med. *336*, 1131–1141.

Park, S.K., Kim, J., Seomun, Y., Choi, J., Kim, D.H., Han, I.O., Lee, E.H., Chung, S.K., and Joo, C.K. (2001). Hydrogen peroxide is a novel inducer of connective tissue growth factor. Biochem. Biophys. Res. Commun. *284*, 966–971.

Rahman, I., Kode, A., and Biswas, S.K. (2006). Assay for quantitative determination of glutathione and glutathione disulfide levels using enzymatic recycling method. Nat. Protoc. *1*, 3159–3165.

Roger, V.L. (2013). Epidemiology of heart failure. Circ. Res. *113*, 646–659.

Rydström, J. (2006). Mitochondrial NADPH, transhydrogenase and disease. Biochim. Biophys. Acta *1757*, 721–726.

Schriner, S.E., Linford, N.J., Martin, G.M., Treuting, P., Ogburn, C.E., Emond, M., Coskun, P.E., Ladiges, W., Wolf, N., Van Remmen, H., et al. (2005). Extension of murine life span by overexpression of catalase targeted to mitochondria. Science *308*, 1909–1911.

Sheeran, F.L., Rydström, J., Shakhparonov, M.I., Pestov, N.B., and Pepe, S. (2010). Diminished NADPH transhydrogenase activity and mitochondrial redox regulation in human failing myocardium. Biochim. Biophys. Acta *1797*, 1138–1148.

Simon, M.M., Greenaway, S., White, J.K., Fuchs, H., Gailus-Durner, V., Wells, S., Sorg, T., Wong, K., Bedu, E., Cartwright, E.J., et al. (2013). A comparative phenotypic and genomic analysis of C57BL/6J and C57BL/6N mouse strains. Genome Biol. *14*, R82.

Smith, R.A., Hartley, R.C., Cochemé, H.M., and Murphy, M.P. (2012). Mitochondrial pharmacology. Trends Pharmacol. Sci. *33*, 341–352.

Starkov, A.A., and Fiskum, G. (2003). Regulation of brain mitochondrial H2O2 production by membrane potential and NAD(P)H redox state. J. Neurochem. *86*, 1101–1107.

Szeto, H.H. (2014). First-in-class cardiolipin-protective compound as a therapeutic agent to restore mitochondrial bioenergetics. Br. J. Pharmacol. *171*, 2029–2050.

Toye, A.A., Lippiat, J.D., Proks, P., Shimomura, K., Bentley, L., Hugill, A., Mijat, V., Goldsworthy, M., Moir, L., Haynes, A., et al. (2005). A genetic and physiological study of impaired glucose homeostasis control in C57BL/6J mice. Diabetologia *48*, 675–686.

Wagner, S., Rokita, A.G., Anderson, M.E., and Maier, L.S. (2013). Redox regulation of sodium and calcium handling. Antioxid. Redox Signal. *18*, 1063–1077.

Wencker, D., Chandra, M., Nguyen, K., Miao, W., Garantziotis, S., Factor, S.M., Shirani, J., Armstrong, R.C., and Kitsis, R.N. (2003). A mechanistic role for cardiac myocyte apoptosis in heart failure. J. Clin. Invest. *111*, 1497–1504.